12th IFAC International Symposium on
Advanced Control of Chemical Processes
July 14-17, 2024. Toronto, Canada

Model-based feedback control of filament geometry in extrusion-based additive manufacturing. ⋆

Carlos J.G. Rojas * **Christian Portilla** * **Leyla Özkan** *,**

* *Eindhoven University of Technology, The Netherlands (e-mail: {c.j.gonzalez.rojas, c.r.portilla, l.ozkan}@tue.nl)*
** *Delft University of Technology, The Netherlands*

Abstract: Control of extrusion-based printing is fundamental to improving the traditional open-loop operation of commercial machines. However, the literature on feedback control based on nozzle motion is still limited in comparison with the developments for extrusion dynamics. In this work, we propose a model-based control strategy where the effects of the nozzle speed on the filament width are described by a first-order model, and the model uncertainty is used for robust synthesis. The feedback employs the internal model controller (IMC) to get an approximate inversion of the dynamics and the IMC filter is tuned based on robust performance criteria. The controller was experimentally tested and provided satisfactory results, especially when the parameters were refined depending on the speed regime.

Keywords: Additive manufacturing, Time delay systems, Advanced process control, Robust control applications, Process control applications.

1. INTRODUCTION

Extrusion-based additive manufacturing (EB-AM) has gained popularity as a method for layer-by-layer building of three-dimensional parts due to its simplicity and material flexibility. Over the past ten years, the EB-AM technology has had remarkable advancements to cover a wide range of printing materials such as ceramics, biomaterials, food, and cement (Altıparmak et al. (2022)). However, most commercial 3D printers still operate in an open-loop mode relying on calibration approaches due to the material's variability. Since the operation is still inefficient, modeling and controlling EB-AM are crucial to make it a viable and robust on-demand production technique.

Extrusion-based printing consists of two dynamically distinct processes, a fast nozzle motion process and a slow extrusion process. When these processes are not properly integrated, printing errors such as over or under-extrusion degrade the quality of the product (Barton et al. (2011)). Depending on the purpose of the model, the filament geometry can be modeled by the use of distributed or lumped representations. A distributed model is obtained by applying the mass and momentum conservation principles for fluid flow, and by tracking the free surface of the build material along the print bed. Distributed models are commonly used for sensitivity analysis of the cross-sectional shape as a function of the nozzle and extrusion speeds (Balta and Altınkaynak (2022); Comminal et al. (2020)). However, the incompressible flow and the stokes assumptions employed in these studies constrain the resulting model to a memoryless behavior. These models do not capture the transient behavior of the build material during important steps such as start and stop operations. In contrast, lumped models have been successfully used in control applications, without the need for costly computational schemes. For control purposes, several works (Hoelzle et al. (2008); Armstrong et al. (2021)) have concluded that the dynamics can be approximated by first-order models, despite the nonlinear extrusion behavior.

Geometry control of EB-AM processes has been focused on manipulating the flow rate, force, and extrusion speed to achieve better operational conditions (Altıparmak et al. (2022)). Model-based strategies have been considered with the purpose of improving the nozzle and extrusion speed integration. For example, in Armstrong et al. (2021), an input-output model was employed to reduce the build-up of material at turnarounds. In addition, the characterization of the dead time helped to trigger the change of the manipulated variable at an appropriate position. Similarly, the work of Wu et al. (2021) proposed two feedforward strategies to reduce defects and increase the dimensional accuracy of printed parts. In one of their approaches, the authors employed a model for the nozzle instead of the extruder speed, as a way to counteract the nonlinearities observed in the process. However, the performance of feedforward approaches for control can be notably more affected by the accuracy of the model employed and the process and measurement noise in comparison to a feedback control strategy. For that reason, we propose a robust model-based feedback control to account for the variability characteristic of EB-AM processes. The internal model controller (IMC) structure applied is advantageous because when the model accuracy is high, it provides a quasi-optimal control strategy based on the inversion of the plant dynamics. Furthermore, IMC handles time delays in a sys-

⋆ This work has been developed as part of the PRINTYOURFOOD project, which is financially supported by the NWO grant number 18763

tem due to the use of the plant model. The control strategy is implemented on a commercial 3D printer employing a non-Newtonian build material. The performance of the controller in terms of the model variability and the IMC filter is analyzed based on the experimental results.

The paper is organized as follows: Section 2 provides an overview of the experimental setup. Section 3 examines the lumped deposition models and the empirical model considered in this study. Section 4 explains the procedure followed for the robust model-based control design. Finally, section 5 contains the experimental results, where the controller performance is analyzed, and section 6 presents the conclusion of this work.

2. EXPERIMENTAL SETUP

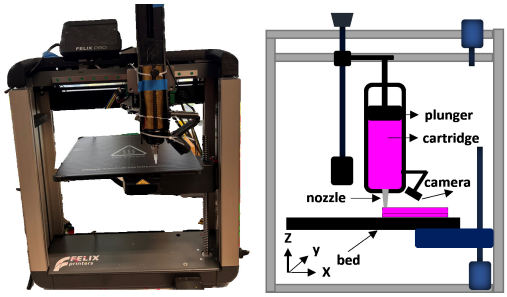

(a) (b)

Fig. 1. (a) Extrusion-based 3D printer. (b) Schematic representation

The 3D printer depicted in Figure 1 is employed to validate the control strategy proposed. The extrusion system consists of a plunger that pushes the ink in the cartridge towards the nozzle. The ink used is commercial Play-Doh (in two bright colors), which is primarily composed of water, salt, and flour. This material is a shear-thickening non-Newtonian fluid (Buechley and Ta (2023)), but the rheological properties are not considered in this work. From a control perspective, the controlled variable is the width of the printed filament (w_f) and the possible manipulated variables are the nozzle speed ($\bar{v}_n$) and the plunger (i.e. extrusion) speed ($\bar{v}_p$). The nozzle speed sets the relative XY motion speed between the nozzle and the bed. In contrast, the plunger speed $\bar{v}_p$ is determined by dividing the plunger displacement (defined in the G-code) by the time required to complete a given XY motion of the head. This means that, due to the machine settings, $\bar{v}_p$ is dependent on the $\bar{v}_n$ selected. In this study, we focus on the role of the nozzle speed as the manipulated variable by keeping the plunger speed constant.

2.1 Vision and communication systems

The sensor is a webcam attached to the head of the printer and directed at the nozzle's tip. The camera collects data to estimate the filament's width on the first layer and has a resolution of 1920x1080 pixels and a sampling rate of 30 fps. The pixels-to-mm conversion factor is $0.17\,mm$. The computer vision algorithm takes the frames collected by the camera, smooths the images, and determines the filament's edges. The start and end coordinates of the edges are estimated by applying the probabilistic Hough transform. Lastly, the width is computed as the perpendicular distance between the center coordinates of the detected edges. The vision system was implemented in Python using the OpenCV library.

The system is actuated by stepper motors through a Duet 2 mainboard. The communication between the controller algorithm and the mainboard was implemented using the Python socket's module. This allows sending and receiving commands via the telnet network protocol. The controller is implemented using ControlDesk (dSPACE software) and MATLAB Simulink.

3. DEPOSITION MODEL

Lumped models establish a relationship between the driving input of extrusion (e.g. plunger pressure or speed) and deposition (nozzle speed) and the filament cross-sectional shape without considering the spatial dependence characteristic of distributed models, as illustrated in Figure 2.

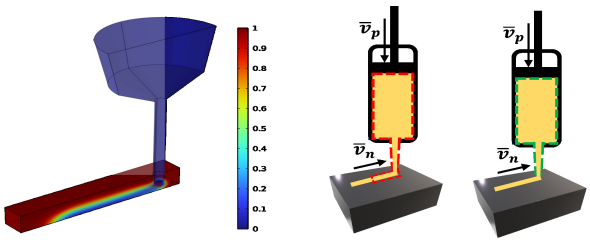

(a) (b) (c)

Fig. 2. (a) Distributed model. (b) Control volume for memoryless behavior. (c) Control volume for dynamic behavior

The simplest model possible, that accounts for the extrusion and deposition phenomena, is determined by assuming incompressibility and applying mass conservation in the control volume (red dotted line) presented in Figure 2b, as follows:

$$\rho Q_{in} = \rho Q_{out} \tag{1}$$

$$Q_{in} = \bar{v}_p A_{in} \tag{2}$$

$$Q_{out} = \bar{v}_n A_{out} \tag{3}$$

Equation (1) is the mass conservation in terms of density ρ and volumetric flow rate Q. Equation (2) provides the inlet flow rate when the driving input is the speed of the plunger $\bar{v}_p$. Equation (3) gives the flow rate at the outlet as the product of the nozzle speed $\bar{v}_n$ and the filament cross-sectional area. This modeling approach has been adopted in EB-AM of different materials (Bonatti et al. (2021); Comminal et al. (2020)), and is implicitly assumed in some 3D printing software to calibrate the ratio between the nozzle and extrusion speeds $\frac{\bar{v}_n}{\bar{v}_p}$. Nevertheless, the resulting memoryless behavior does not consider the influence of previous states or the rheology of the material, which limits its control applications.

3.1 Dynamic modeling

A dynamic model can be developed by assuming flow compressibility due to the properties of the build material and the fluid reservoir. For example, in Hoelzle et al. (2008)

a nonlinear flow-pressure relationship considering the rheological effects on the outlet flow was proposed. Considering the control volume (green dotted line) illustrated in Figure 2c, the model relates the top and bottom volumetric flow rates to the pressure of the fluid P_r as follows:

$$V_r \alpha_i \left(P_r\right)^{1-\frac{1}{n}} \dot{Q}_{out} + Q_{out} = Q_{in} \tag{4}$$

where V_r is the volume of ink in the cartridge, α_i and n are constants that account for the rheological properties and Q_{in} is given by (2). After linearization of (4) about a nominal V_r and P_r, the next first order model is derived:

$$\tau \dot{Q}_{out} + Q_{out} = K \bar{v}_p \tag{5}$$

where K is the steady-state gain which provides the response of the system after the dynamic effects have vanished. In steady-state, (5) simplifies to (1) with $K = A_{in}$. The parameter τ, known as the time constant, gives a measure of the speed of response and is a function of the reference values used for linearization. The filament width w_f can be related to the outlet flow Q_{out} by using (3) and assuming a constant cross-section. For example, if an ellipsoidal shape is considered, $A_{out} = \pi w_f h$, where w_f and h are the width and height of the filament cross-section (Armstrong et al. (2021)). As w_f and Q_{out} are proportionally related, then a first-order model can be directly fitted considering w_f as the output.

If (3) is employed directly in (1), it is assumed that there is only a memoryless effect of $\bar{v}_n$ on w_f. As a result, the dynamic effects of the nozzle speed $\bar{v}_n$ on the width are not considered. However, the filament shape is also affected by changes in $\bar{v}_n$, which, depending on the process conditions, could have a faster effect on its formation. Compensation using nozzle speed has been applied especially for material deposition at corners. Undesired features, such as swelling, can be corrected by modifying the nozzle deceleration and acceleration profiles(Comminal et al. (2019)). However, to the best of our knowledge, for a reference tracking control application only the work of Wu et al. (2021) has employed a first-order empirical model to describe the effects of the nozzle speed.

In this work, we consider a first-order plus dead-time model (FOPDT) for the deposition dynamics:

$$G(s) = \frac{w_f(s)}{\bar{v}_n(s)} = \frac{K e^{-\theta s}}{\tau s + 1} \tag{6}$$

FOPDT models represent the sigmoidal shape of the step response obtained in many process applications and can capture higher-order behaviors when the system has a dominant pole. The addition of an output delay of the form $w_f^* = w_f(t-\theta)$ is included to represent the time $\theta > 0$ taken by communication and sensing delays.

3.2 Parametric estimation from step response

A FOPDT model is used to relate the effect of the input ($\bar{v}_n$) to the output (w_f). The time domain response for a step input of size Δv_n is given by:

$$w_f(t) = \begin{cases} 0 & t < \theta \\ K \Delta v_n \left(1 - e^{-\frac{t-\theta}{\tau}}\right) & t \geq \theta \end{cases} \tag{7}$$

The steady-state gain can be computed from:

$$K = \frac{w_f(t \to \infty) - w_f(t=0)}{\Delta v_n} \tag{8}$$

and after preprocessing the data, θ and τ can be determined by using the analytical time domain solution (7) as follows:

$$\theta - ln\left(1 - \frac{w_f(t=t_n)}{w_f(t \to \infty)}\right)\tau = t_n \tag{9}$$

Thus, by using several combinations of two samples ($n = 1, 2$) along the transient part of the experimental step-response $w_f(t)$, the parameters (θ, τ) can be estimated.

4. MODEL-BASED CONTROL DESIGN

The objective of a model-based approach is to synthesize the controller based on the available mathematical model of the system. In addition, the controller structure is not restricted to standard techniques such as PID. We consider a feedback internal model control (IMC) where the model input is the manipulated variable $\bar{v}_n$ and its output is an estimate of w_f. The IMC is equivalent to the Smith's predictor structure, which untangles the dead-time from the control loop (Kravaris and Kookos (2021)).

4.1 Robust internal model control (IMC) for a FOPDT system

We use the procedure proposed in Kravaris and Kookos (2021); Morari and Zafiriou (1989) to synthesize an IMC scheme accounting for robust stability and performance. The specifications are to design a system with no offset for step changes of the set point (w_{sp}). All three parameters of the model are considered to be uncertain:

$$\begin{aligned} K_l \leq K \leq K_u \\ \tau_l \leq \tau \leq \tau_u \\ \theta_l \leq \theta \leq \theta_u \end{aligned} \tag{10}$$

where the sub-indices l and u represent the lower and upper limits and the nominal plant $\tilde{G}$ is defined by the mean parameters $(\tilde{K}, \tilde{\theta}, \tilde{\tau})$. Thus, the family of plants considered for robust design is given by:

$$\Pi = \left\{ G : \left| \frac{G(j\omega) - \tilde{G}(j\omega)}{\tilde{G}(j\omega)} \right| \leq \bar{L}_m(\omega) \right. \tag{11}$$

with members defined by the multiplicative uncertainty L_m as follows:

$$G(j\omega) = \tilde{G}(j\omega)(1 + L_m(j\omega)), \quad |L_m(\omega)| \leq |\bar{L}_m(\omega)| \tag{12}$$

The nearly optimal controller, which minimizes the integral of the squared error (ISE), is computed by decomposing $\tilde{G}(s)$ into the following product:

$$\begin{aligned} \tilde{G}(s) &= \tilde{G}_A(s)\tilde{G}_M(s) \\ \tilde{G}_A(s) &= e^{-\tilde{\theta}s} \\ \tilde{G}_M(s) &= \frac{\tilde{K}}{\tilde{\tau}s + 1} \end{aligned} \tag{13}$$

Next, a type 1 filter $F(s)$ is used to make $\tilde{Q}(s) = \tilde{G}_M^{-1}$ proper, and the equivalent controller transfer function $G_c(s)$ realizable:

$$G_c(s) = \frac{1}{\lambda s + 1 - e^{-\tilde{\theta}s}} \frac{\tilde{\tau}s + 1}{\tilde{K}} \tag{14}$$

A block diagram representing the IMC controller (dotted box) is shown in Figure 3. Finally, the filter constant λ is

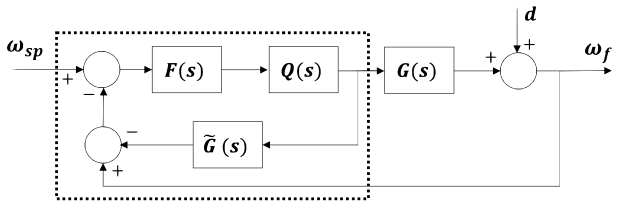

Fig. 3. Block diagram IMC controller

determined based on the robust constraints:

$$\left|F\bar{L}_m\right| < 1 \tag{15}$$

$$\left|F\bar{L}_m\right| + \left|(1 - e^{-j\omega\tilde{\theta}}F)W\right| < 1 \tag{16}$$

where $\left|\tilde{G}\tilde{Q}\right| = \left|e^{-\tilde{\theta}s}\right| = 1$ has been used to simplify the expressions and W is the performance weight. For simplicity, the peak of the sensitivity function $S = (1 - \tilde{G}\tilde{Q}F)$ is used to define the performance weight $W^{-1} = \max_{\omega} |S(j\omega)|$. We see that robust performance (16) implies robust stability (15) , and therefore (16) is used to tune the filter constant λ.

5. EXPERIMENTAL RESULTS

In this section, we present the results of applying the proposed model-based control design on the experimental setup described in section 2. Both the estimation and control experiments were performed using a reference speed $\bar{v}_{ref} = 10\,mm/s$. The manipulated variable is the nozzle speed $\bar{v}_n$, but the results are presented in terms of the speed factor $F_n = \frac{\bar{v}_n}{\bar{v}_{ref}}$.

5.1 FOPDT model parameter estimation

The estimation experiments were designed to have a calibration stage where the flow is initiated, followed by a printing pattern with 4 intermediate and 4 experiment lines. An intermediate line is printed before every experiment line and set with the same printing parameters to establish similar initial conditions between experiments. A picture of samples for a F_n step change of 0.2 and 2.0 is shown in Figure 4a. The head of the printer moves for a travel distance of $180\,mm$, and when the nozzle is located at $x = 60\,mm$ a speed factor change is commanded. The speed factors considered during the estimation experiments are $(0.2, 0.4, 0.6, 0.8)$ and $(1.2, 1.4, 1.6, 1.8, 2.0)$ for a decrease and increase in the speed respectively. Due to the nonlinear characteristics of the process and the small variations in the fluid flow at least 8 samples for each speed factor were included during the estimation of the parameters. The mean parameter values are estimated based on the normalized behavior of the measured width and the results are presented in Figure 4b. Since the flow is initiated before the experiments, θ is attributed to the communication delays of the system and has a similar value independently of the speed factor. In contrast, τ and K depend on the speed regime, which indicates the nonlinear behavior of the system.

Due to the speed regime dependence observed, we determine three sets of model parameters for the controller, one considering all the speed factors (combined) and the other two regarding the increasing and decreasing speed

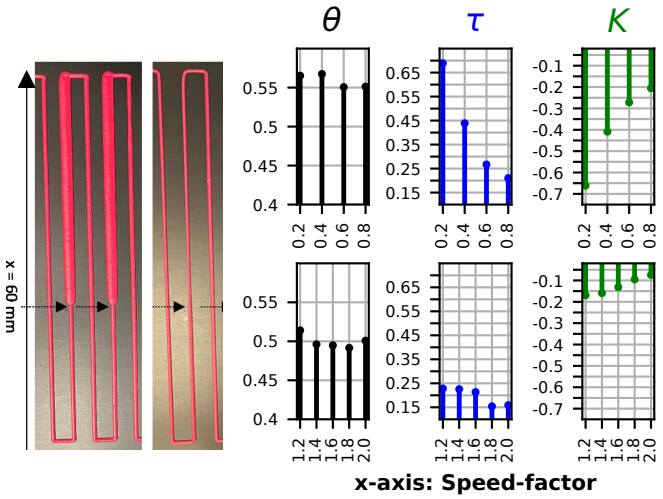

(a) (b)

Fig. 4. (a) FOPDT estimation experiments. (b) Estimated parameters by speed factor.

regimes. The mean value μ and standard deviation σ of the parameters are given in Table 1. The absolute mean values for τ and K in the decreasing speed regime are two and three times higher, respectively, compared to the values in the increasing regime. The high standard deviation of τ and K parameters for the combined regime are the result of the wide range of values observed in Figure 4.

Table 1. Parameters for model-based controller

Speed regime	θ		τ		K	
	μ	σ	μ	σ	μ	σ
Combined	0.53	0.07	0.30	0.11	-0.25	0.18
Increasing	0.50	0.05	0.20	0.08	-0.13	0.06
Decreasing	0.56	0.09	0.40	0.14	-0.38	0.18

5.2 Robust IMC controller

As explained in section 4, the filter parameter λ for the IMC controller is determined from the robust performance condition (16). $\bar{L}_m$ is defined based on the mean parameter values and their upper and lower limits in (10). We define the limits of the parameters by assuming a normal distribution and using the relationship $\mu \pm 2\sigma$ to cover the wide range of data. The performance weight condition is selected to be $W^{-1} = 2.0$ and the filter values computed for the different regime conditions are given in Table 2. The specification of W is based on the maximum peak of

Table 2. λ based on the speed regime

Combined	Increasing	Decreasing
$\lambda = 1.2$	$\lambda = 1.1$	$\lambda = 1.78$

the sensitivity function which is typically required to be smaller than 0.9.

We ran different experimental repetitions to evaluate the performance of the controller based on the error and the speed factor dynamics. The control experiments start with the calibration stage where the flow is initiated, but only one set of intermediate-experiment lines is printed in every repetition. Since the model parameters are computed using

the normalized response, the model and the setpoint are in terms of deviations from the initial width, and the manipulated variable is in terms of the reference speed. The initial width ω_0 of each experiment is computed by taking an average of the measured width before the setpoint change and it is provided with the results.

5.3 Feedback control for setpoint tracking - Decreasing step change

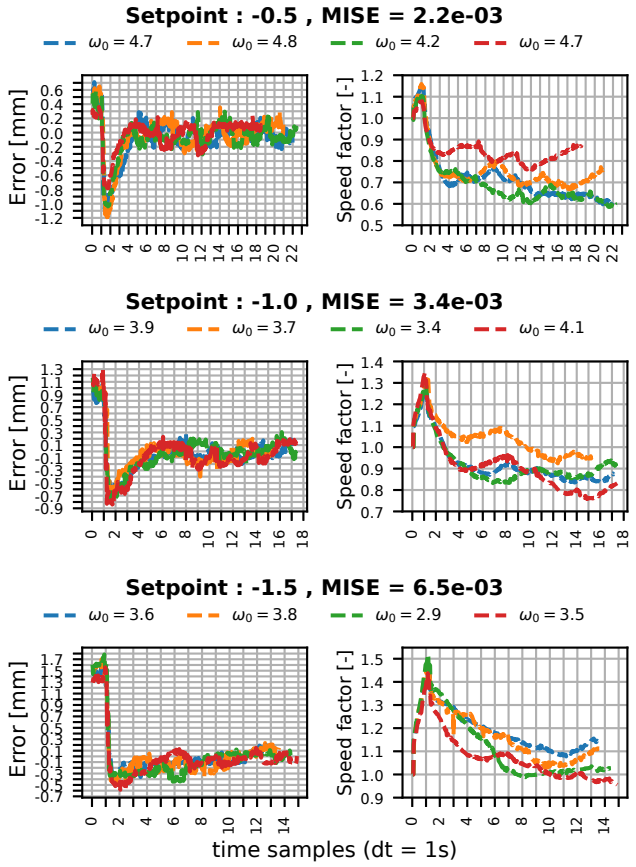

Fig. 5. Error dynamics for decreasing setpoint step change

For this step change, a lower nozzle reference speed in the intermediate line was required to have a sufficiently wider filament. The results using the filter parameter from the combined regime for three different setpoint changes are shown in Figure 5. In most cases, the error has an overshoot between 1 and 2.5 s after the setpoint is changed. The curves get within a margin of $\pm 0.2\,mm$ after $12\,s$ which can be attributed to the sensor resolution (pixel-to-mm conversion factor of $0.17\,mm$). The mean integral squared error (MISE) has a positive correlation with the size of the setpoint step and is dominated by the system's transient response, especially by the signal overshoot. The controller with λ from the combined regime showed slightly better performance than the one from the increasing speed regime, which is logical considering that the speed factor moves up and down from the reference speed.

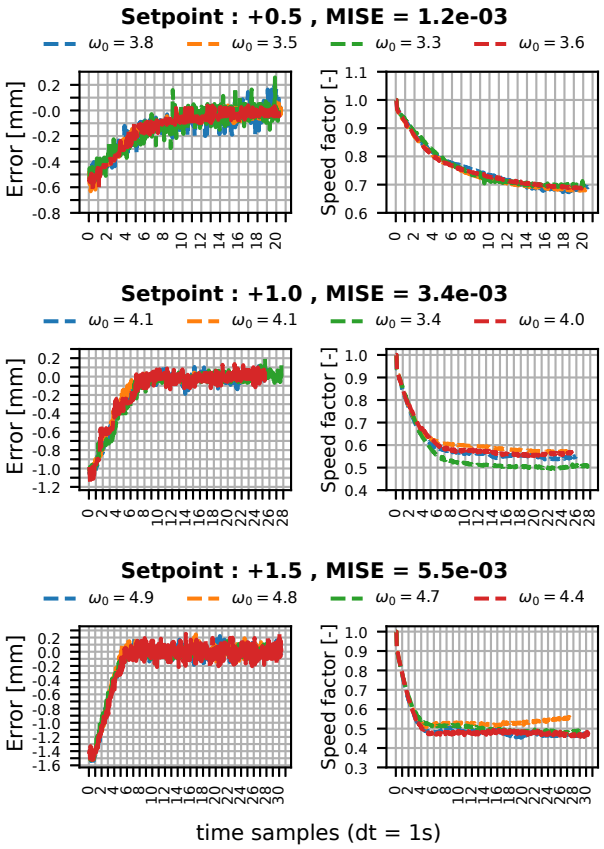

Fig. 6. Error dynamics for increasing setpoint step change

5.4 Feedback control for setpoint tracking - Increasing step change

The results using λ from the decreasing speed regime for three different set point changes are given in Figure 6. The error does not have an overshoot and it gets within a margin of $\pm 0.2\,mm$ after $10\,s$. Due to the slower transient response, the MISE is only slightly smaller in comparison with the decreasing setpoint test. We also tested the controller with the filter from the combined speed regime but noticed that the performance was notably degraded. This happened especially when the speed factor reached values below 0.4.

5.5 Feedback control for setpoint tracking - Filter parameter effects

Finally, we tested the effect of the filter parameters on the system's performance for an increasing step change of $1.5\,mm$. We compared the λ determined from the decreasing regime performance against the value obtained from the robust stability condition $\lambda = 0.5$ (based on (15)). Additionally, a parameter in between the robustness conditions $\lambda = 0.9$ was also considered. Figure 7 exhibits the system's dynamics for every parameter and 4 experimental repetitions. It can be seen that with the decrease in the filter parameter, the controller reaction is more aggressive. For this reason, we calculated the MISE after 5 seconds to evaluate the performance after the initial transient effects had vanished. In this case, the MISE for $\lambda = 1.78$ is about an order of magnitude smaller than for $\lambda = 0.5$. For $\lambda = 0.9$ we see that in one repetition this led to small

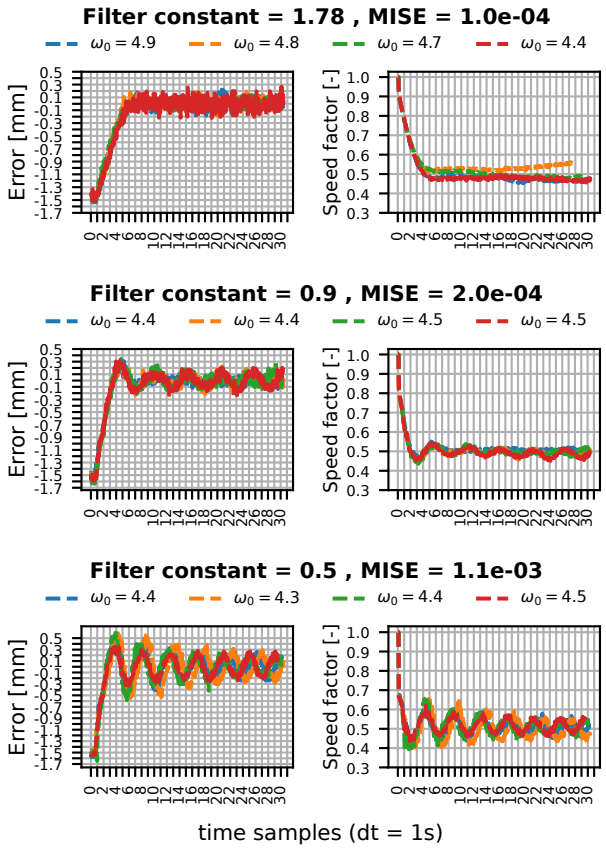

Fig. 7. Filter parameter effects on performance

oscillations around 0, while for $\lambda = 0.5$ all the repetitions had a similar oscillatory behavior, which might indicate that the model uncertainty is too high to ensure robust stability. The qualitative differences in the filament shape are illustrated in Figure 8, where it is clearly seen the width variation between the 3 different IMC filters.

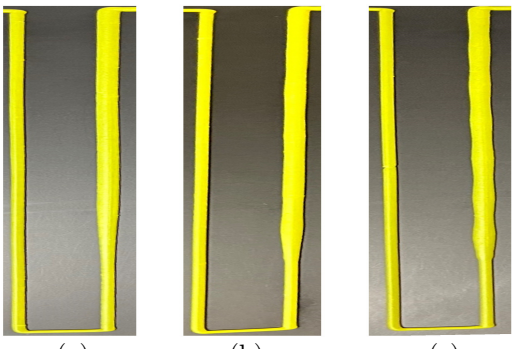

(a) (b) (c)

Fig. 8. Filter effects on filament shape. (a) $\lambda = 1.78$. (b) $\lambda = 0.9$. (c) $\lambda = 0.5$.

6. CONCLUSIONS

In this work, we have proposed a robust model-based design for the filament geometry control in extrusion-based printing. The nonlinear behavior of the filament width to changes in the nozzle speed has been approximated by a FOPDT model. Several open-loop step response experiments were conducted and the analysis of the model parameters showed significant variations depending on whether the speed factor is increased or decreased. This had some implications for the controller's performance. Depending on the direction of the setpoint change, the IMC model can be refined for a specific speed factor regime as was the case for the increasing setpoint change test. This refinement of the FOPDT parameters, especially of the steady-state gain, provided smoother responses without overshoot, reaching a steady state within the measurement resolution. Nevertheless, when the speed factor reaches low values, the model uncertainty might be too high to guarantee a robust performance. For cases such as the decreasing setpoint change, nonlinear control strategies and the inclusion of constraints on the manipulated variable should also be considered in the control design.

REFERENCES

Altıparmak, S.C., Yardley, V.A., Shi, Z., and Lin, J. (2022). Extrusion-based additive manufacturing technologies: State of the art and future perspectives. *Journal of Manufacturing Processes*, 83, 607–636.

Armstrong, A.A., Pfeil, A., Alleyne, A.G., and Wagoner Johnson, A.J. (2021). Process monitoring and control strategies in extrusion-based bioprinting to fabricate spatially graded structures. *Bioprinting*, 21.

Balta, E.C. and Altınkaynak, A. (2022). Numerical and experimental analysis of bead cross-sectional geometry in fused filament fabrication. *Rapid Prototyping Journal*, 28(10), 1882–1894.

Barton, K.L., Hoelzle, D.J., Alleyne, A.G., and Johnson, A.J.W. (2011). Cross-coupled iterative learning control of systems with dissimilar dynamics: design and implementation. *International Journal of Control*, 84(7), 1223–1233.

Bonatti, A.F., Chiesa, I., Vozzi, G., and De Maria, C. (2021). Open-source CAD-CAM simulator of the extrusion-based bioprinting process. *Bioprinting*, 24.

Buechley, L. and Ta, R. (2023). 3D Printable Play-Dough: New Biodegradable Materials and Creative Possibilities for Digital Fabrication. In *Proceedings of the 2023 CHI Conference on Human Factors in Computing Systems*, 1–15. ACM, Hamburg Germany.

Comminal, R., Leal Da Silva, W.R., Andersen, T.J., Stang, H., and Spangenberg, J. (2020). Modelling of 3D concrete printing based on computational fluid dynamics. *Cement and Concrete Research*, 138.

Comminal, R., Serdeczny, M.P., Pedersen, D.B., and Spangenberg, J. (2019). Motion planning and numerical simulation of material deposition at corners in extrusion additive manufacturing. *Additive Manufacturing*, 29.

Hoelzle, D.J., Alleyne, A.G., and Wagoner Johnson, A.J. (2008). Iterative learning control for robotic deposition using machine vision. In *2008 American Control Conference*, 4541–4547.

Kravaris, C. and Kookos, I.K. (2021). *Understanding Process Dynamics and Control*. Cambridge Series in Chemical Engineering. Cambridge University Press.

Morari, M. and Zafiriou, E. (1989). *Robust process control*. Prentice Hall, Englewood Cliffs, N.J.

Wu, P., Ramani, K.S., and Okwudire, C.E. (2021). Accurate linear and nonlinear model-based feedforward deposition control for material extrusion additive manufacturing. *Additive Manufacturing*, 48.